

X-RAYS FROM A RADIO-LOUD COMPACT BAL QUASAR 1045+352 AND THE NATURE OF OUTFLOWS IN RADIO-LOUD BAL QUASARS

MAGDALENA KUNERT-BAJRASZEWSKA¹, ANETA SIEMIGINOWSKA², KRZYSZTOF KATARZYŃSKI¹, AGNIESZKA JANIUK³

¹ Toruń Centre for Astronomy, N. Copernicus University, Gagarina 11, 87-100 Toruń, Poland

² Harvard Smithsonian Center for Astrophysics, 60 Garden St, Cambridge, MA 02138 and

³ N. Copernicus Astronomical Center, Bartycka 18, 00-716 Warsaw, Poland

February 7, 2020

ABSTRACT

We present new results on X-ray properties of radio loud broad absorption line (BAL) quasars and focus on broad-band spectral properties of a high ionization BAL (HiBAL) compact steep spectrum (CSS) radio-loud quasar 1045+352. This HiBAL quasar has a very complex radio morphology indicating either strong interactions between a radio jet and the surrounding interstellar medium or a possible re-start of the jet activity. We detected 1045+352 quasar in a short 5 ksec *Chandra* ACIS-S observation. We applied theoretical models to explain spectral energy distribution (SED) of 1045+352 and argue that non-thermal, inverse-Compton emission from the innermost parts of the radio jet can account for a large fraction of the observed X-ray emission. In our analysis we also consider a scenario in which the observed X-ray emission from radio-loud BAL quasars can be a sum of inverse-Compton jet X-ray emission and optically thin corona X-ray emission. We compiled a sample of radio-loud BAL quasars that were observed in X-rays to date and report no correlation between their X-ray and radio luminosity. However, the radio-loud BAL quasars show a large range of X-ray luminosities and absorption columns. This is consistent with the results obtained earlier for radio-quiet BAL quasars and may indicate an orientation effect in BAL quasars or more complex dependence between X-ray emission, radio emission and an orientation based on the radio morphology.

Subject headings: quasars: absorption lines — quasars: general — X-rays: galaxies

1. INTRODUCTION

About 10-30% of quasars population show blueshifted broad absorption lines (BALs) of the high ionization resonant lines (CIV 1549Å – high-ionization BAL (HiBAL) quasars). 10% of them also show absorption troughs in low ionization lines (MgII 2800Å – low-ionization BAL (LoBAL) quasars). BALs are probably caused by the outflow of gas with velocities up to 0.2c (Hewett & Foltz 2003) and are associated with the accretion process. As it has been recently found (Becker et al. 2000) both radio-quiet and radio-loud quasars can have BALs. There are two scenarios explaining origin and nature of BAL quasars. According to the first one, BAL regions exist in both BAL and non-BAL quasars, and the BAL quasars are normal quasars seen along a particular line of sight - at high inclination angles (Murray et al. 1995; Elvis 2000). The second says that BALs may be associated with a short-lived evolutionary quasar phase characterized by a large covering fraction wind, rather than the orientation (Gregg et al. 2000, 2006).

Theoretical models (Murray et al. 1995; Elvis 2000) suggest that BALs are seen at high inclination angles, which means that the outflows from accretion disks are present near an equatorial plane. However, some recent numerical work indicates that it is also plausible to launch bipolar outflows from the inner regions of a thin disk (e.g. Ghosh & Punnsly 2007; Proga & Kallman 2004). There is a growing observational evidence indicating the existence of polar BAL outflows (e.g. Zhou et al. 2006; Ghosh & Punnsly 2008). This means that there is no one simple orientation model which can explain all the features observed in BAL quasars.

X-ray observations of radio-quiet BAL quasars

(Green et al. 2001; Gallagher et al. 2006) indicate that they are X-ray weak, perhaps due to a high absorption column intrinsic to the source. Their X-ray spectra display a clear evidence of X-ray absorption, often complex, with high intrinsic column densities $N_H > 10^{22}$ cm⁻² (Gallagher et al. 2002). The origin of the BAL X-ray absorber is still debated, although a broadening of the optical absorption lines suggest the high velocity outflows as a source of this absorption. This view was challenged by Giustini et al. (2008) and Shen et al. (2008) who concluded that X-ray selected BALs appear less X-ray absorbed than purely optically selected ones. This could be a geometrical effect: we observe these objects at smaller angles with respect to the accretion disk rotation axis, so missing the bulk of X-ray shielding gas and the highest outflow velocities.

Radio band observations can provide orientation information for radio-loud quasars with BALs, so chances to study and identify the origin of the absorbing gas are higher in the radio-loud than in the radio-quiet quasars. In addition radio-loud quasars are more X-ray loud than the radio-quiet quasars (Young et al. 2009). However, X-ray observations of radio-loud BALs are sparse and only a handful of them have been observed in X-rays so far (Brotherton et al. 2005; Miller et al. 2006; Schaefer et al. 2006; Wang et al. 2008, and this paper). There is also a very limited information about the radio morphology of BAL quasars. There are only ten of them with known large scale radio morphology (Wills et al. 1999; Gregg et al. 2000, 2006; Brotherton et al. 2002; Zhou et al. 2006). Most of the radio-loud BAL quasars detected to date have very compact radio structures similar to Gigahertz-Peaked Spec-

trum (GPS) and Compact Steep Spectrum (CSS) sources which are thought to be young (O’Dea 1998). There are only a few radio-loud compact BAL quasars with resolved structures that were observed in radio band at one frequency only (Jiang & Wang 2003; Liu et al. 2008). The first multifrequency radio observations of a very compact HiBAL quasar 1045+352 were made by Kunert-Bajraszewska & Marecki (2007). The complex compact structure has been resolved into many sub-components and indicates that the jet is moving in a non-uniform way in the central regions of the host galaxy.

We observed 1045+352 BAL quasar ($z = 1.604$) in X-rays using *Chandra* X-ray Observatory. We report the results of this observation in Sec. 2, present and model the spectral energy distribution of 1045+352 in Sec. 3 and discuss the source properties together with the properties of all radio-loud BAL quasars observed to date in Sec. 4. Finally Sec. 5 summarises the main conclusions.

Throughout the paper, we assume a cosmology with $H_0 = 71 \text{ km s}^{-1} \text{ Mpc}^{-1}$, $\Omega_M = 0.27$, $\Omega_\Lambda = 0.73$.

2. CHANDRA X-RAY OBSERVATION

1045+352 BAL quasar was observed with the *Chandra* Advanced CCD Imaging Spectrometer (ACIS-S, Garmire et al. 2003) on 2008 Jan 20 (ObsID 9320). The source was located at the default aim-point position on the ACIS-S backside illuminated chip S3 (Proposer’s Observatory Guide (POG)¹). The 1/8 subarray CCD readout mode of one CCD only was used resulting in 0.441 sec frame readout time. The effective exposure time for this observation was 4658.44 sec.

We observed 5 counts in the assumed 1.3 arcsec radius circular source region defined at the position of the radio source (Table 1). All the detected counts are within the 0.5-7 keV energy range. We calculated the significance of this detection assuming the Poisson distributions for the source and background. Given 6 background counts in the background region (~ 50 times larger than the source region) and assuming the Poisson background we simulated the expected background count rate in the source region. This simulation accounts for the fluctuations in the background. We obtained the significance of observing 5 counts given the background rate at 6×10^{-7} and concluded that the detection of the source is highly significant.

The observed 5 counts give a source flux within 0.5-7 keV of $1.25_{-0.58}^{+0.37} \times 10^{-14} \text{ erg cm}^{-2} \text{ s}^{-1}$ assuming a power law model with $\Gamma = 1.7$ and absorption at $z = 0$ of $N_H = 1.28_{-0.7}^{+1.06} \times 10^{22} \text{ cm}^{-2}$ (the errors are 1σ for 1 significant parameter). The absorption column is treated as an observed minimal value of the absorption in this source and the calculated source flux we take into account in SED modelling. The absorption column was obtained in Sherpa by fitting an absorbed power law model with fixed photon index assuming Cash statistics and it is only a rough approximation as the true value of the continuum shape is unknown. We derive the 3 sigma upper limit on the intrinsic absorber at $z = 1.604$ of $N_H < 9.6 \times 10^{23} \text{ cm}^{-2}$. The unabsorbed X-ray flux in the 0.5-7 keV band assuming only Galactic absorption and photon index $\Gamma = 1.7$ is $7.00 \times 10^{-15} \text{ erg cm}^{-2} \text{ s}^{-1}$.

We calculated the observed hardness ratio for the

source: $HR = (H - S)/(H + S) = 3/5 = 0.6$ (where, $H = \text{Hard}(2-10 \text{ keV}) = 4$ counts; $S = \text{Soft}(0.5-2 \text{ keV}) = 1$ count). The X-ray spectrum appears to be relatively hard, although more counts are needed to confirm this result. Table 1 lists all the observed X-ray and radio parameters for this source.

3. BAL QUASAR 1045+352

1045+352 HiBAL quasar is a compact radio-loud CSS source at redshift $z = 1.604$ (Willott et al. 2002). According to the evolution theory the CSS sources are young AGNs evolving into large scale FRI and FRII radio sources. They probably originate in a merger event and it is possible that in a case of 1045+352 traces of that process are still visible. This HiBAL quasar 1045+352 has a complex radio morphology with a radio jet axis re-orientation: the NE/SW emission can be the first phase of activity, now fading away, and the extension in the NW/SE direction is a signature of the current active phase. Such a reorientation of the jet axis may result from (1) a merger, (2) a jet precession, or (3) jet-cloud interactions (Kunert-Bajraszewska & Marecki 2007). Its high submillimetre emission and a distorted radio structure indicate that the whole source resides inside the dense medium of the host galaxy, which together with the small (4.3 kpc) linear radio size suggest it is a young AGN.

Our *Chandra* X-ray observation of 1045+352 gives a source unabsorbed 2 keV flux of $1.32 \times 10^{-15} \text{ erg cm}^{-2} \text{ s}^{-1} \text{ keV}^{-1}$ assuming a power law model with $\Gamma = 1.7$ and Galactic absorption. The estimated observed $\alpha_{ox} = 1.38$ would indicate a rather normal, unabsorbed radio-loud quasar. However, the optical flux is reddened by $A_V = 1.5$ (Willott et al. 2002). Based on the estimated dereddened optical flux we calculated intrinsic optical-X-ray index, $\alpha_{ox} = 1.88$. This is typical value for radio-quiet quasars, although (Siemiginowska et al. 2008) found the similar values of α_{ox} in a sample of radio-loud GPS and CSS quasars. Note that such high value of α_{ox} may also suggest a presence of an X-ray absorber close/in the BLR region.

3.1. Black Hole Mass Estimation

Using the published optical spectrum and emission line data for 1045+352 (Willott et al. 2002) we estimated its black hole mass and the Eddington luminosity ratio. To estimate the black hole mass we used the following prescription derived by McLure & Jarvis (2002), which uses the 3000Å monochromatic luminosity and the Mg II $\lambda 2800$ FWHM:

$$\frac{M_{\text{BH}}}{M_\odot} = 3.37 \left(\frac{\lambda L_{3000}}{10^{44} \text{ erg s}^{-1}} \right)^{0.47} \left(\frac{\text{FWHM}(\text{Mg II})}{\text{km s}^{-1}} \right)^2 \quad (1)$$

The obtained value is $M_{\text{BH}} = 1 \times 10^8 M_\odot$, which we then used to calculate the Eddington luminosity:

$$L_{\text{Edd}} = 1.25 \times 10^{38} \left(\frac{M_{\text{BH}}}{M_\odot} \right) \text{ erg s}^{-1} \quad (2)$$

We estimated the bolometric luminosity for 1045+352 using the following equation:

$$L_{\text{bol}} = 4\pi D_L^2 f(1+z)\lambda F_\lambda, \quad (3)$$

¹ <http://asc.harvard.edu/proposer/POG/index.html>

where $\lambda = 3000\text{\AA}$ and $f=5$ is the average bolometric correction from 3000\AA (Ganguly et al. 2007). The Eddington luminosity ratio is then: $L_{\text{bol}}/L_{\text{Edd}} = 0.36$. It has to be noted here that the mass estimate based on the MgII emission line width (and so the value of the accretion rate) can have a large error. We treated these values as the input parameters for an accreting corona model of active galactic nuclei described by Janiuk & Czerny (2000) which we used together with the synchrotron self-Compton scenario to model SED of 1045+352.

3.2. Broad-band emission of 1045+352: Models

Broad-band spectra of 1045+352 are characterized by the strong radio emission, peak in the IR, and relatively strong UV-X-ray continuum. We apply two emission models to the observed multiwavelength spectrum of 1045+352. We start with the emission related to the jet, because the quasar is radio-loud and the jet dominates the observed radio emission. In the second step we calculate the contribution to the spectrum from our accretion disk-corona model.

3.2.1. X-ray emission of the jet

Significant or even dominant part of the X-ray emission could be produced by propagating radio jets and expanding lobes, located at the distance a few hundred parsec from the center of the source (Miller et al. 2006; Stawarz et al. 2008). To check this possibility we use a simple model that is able to reproduce the observed spectra.

We assume a spherical geometry of this part of the jet, described by radius R . More complex, conical or paraboloid geometry could better describe this region (e.g. Konigl 1981; Ghisellini et al. 1985), however, such modeling requires more free parameters, which are difficult to constrain from the observations. The spherical region in our model is filled by relativistic electrons and tangled magnetic field characterized by strength B . The electron energy distribution is assumed to be a power-law function $N(\gamma) = K\gamma^{-n}$ for $1 < \gamma \leq \gamma_{\text{max}}$, where γ is the Lorentz factor that describes electron energy ($E = \gamma m_e c^2$), K describes particle density for $\gamma = 1$, and n is the index of the energy spectrum. The relativistic electrons spinning around magnetic field lines produce synchrotron emission. Some fraction of this emission is up-scattered to higher energies by the electrons. This is well known synchrotron self-Compton scenario (SSC). To calculate the synchrotron emission we use the emissivity derived by Crusius & Schlickeiser (1986) and Ghisellini et al. (1988). The inverse-Compton (IC) radiation is calculated using Compton-kernel derived by Jones (1968). The emission produced in the jet comoving frame is transformed to the observer's frame using standard formulae and assumed value of the Doppler factor (δ). However, proper motions of jet's components in CSS objects are relatively slow (up to $0.3c$, Polatidis & Conway 2003). This together with an estimation of the viewing angle (see Table 1) is limiting the Doppler factor to $\delta < 2$ and practically eliminating it as a free parameter.

This is in fact the simplest possible scenario that may explain jet emission in a wide range of energies, starting from low frequency radio observations up to gamma rays. The model requires only three free parameters (R, B, K).

Moreover, the index of the particle energy spectrum (n) can be constrained directly from the observations using fundamental relationship $\alpha_r = (n - 1)/2$, where α_r is the spectral index of the observed synchrotron emission $F_{\text{syn}} \propto \nu^{-\alpha_r}$. The maximum energy of the electrons, characterized by γ_{max} can be derived from the standard formula that describes particle cooling due to the synchrotron and the inverse-Compton emission

$$\gamma_{\text{max}}(t) = \frac{1}{Ct}, \quad C = \frac{4}{3} \frac{\sigma_{TC}}{m_e c^2} (U_B + U_{\text{rad}}), \quad (4)$$

where $U_B = B^2/(8\pi)$ is the magnetic field energy density and U_{rad} is the synchrotron radiation field energy density (i.e. Kardashev 1962). We calculate γ_{max} for the time $t = R/c$, e.g. the minimum travel time across the source. This assumption may overestimate the maximum energy if the cooling process is dominating the particle energy evolution. On the other hand our estimation does not take into account any possible acceleration of the particles that may partially compensate the cooling process.

In our first attempt to fit the observations we assume that the whole emission observed from the radio frequencies up to IR range is produced by a spherical knot of the jet. This assumption gives five direct observational constraints. The first constraint is the self-absorption frequency (ν_s). Some fraction of the low frequency synchrotron emission can be absorbed by the electrons inside the source. This is well known electron self-absorption process that modifies index of the synchrotron emission producing $\alpha_r = 5/2$. In 1045+352 the self-absorption modifies the index of the emission below $\nu_s \simeq 10^8$ Hz. On the other hand, the synchrotron emission of the knot must extend up to the IR range, above 10^{11} Hz. This gives observational constraints for γ_{max} that must be high enough to explain such emission. The levels of the synchrotron and the IC emission give the next two observational constraints. Note that the ratio between the synchrotron and the IC emission directly indicates the ratio between U_B and U_{rad}

$$\frac{U_B}{U_{\text{rad}}} \simeq \frac{F_{\text{peak,syn}}}{F_{\text{peak,IC}}}, \quad (5)$$

where $F_{\text{peak}} = \max[\nu F(\nu)]$. In the case of 1045+352 $F_{\text{peak,syn}} > F_{\text{peak,IC}}$ that shows dominance of the synchrotron cooling over the IC losses. This basically means that the value of γ_{max} is controlled by the magnetic field strength. Finally, the slope of the synchrotron emission gives the fifth observational constraint. We estimated the value of this parameter to be $\alpha_r = 0.8$, that gives $n = 2.6$. The α_r value has been determined using all available radio points and it is slightly different from that presented in Table 1. Taking into account all the above constraints we obtained satisfactory fit (Fig. 1a) using $\delta = 1.3$, $B = 8 \times 10^{-4}$ G, $K = 2.5 \text{ cm}^{-3}$ and $R = 1.1 \times 10^{21}$ cm (356.5 pc). Moreover, we calculated values of $\gamma_{\text{max}} = 2.68 \times 10^4$, $U_{\text{rad}}/U_B = 0.23$ and $E_e/E_B = 1.34 \times 10^2$, where E_e is the total energy of the electrons and E_B is the total energy accumulated in the magnetic field. The last result shows no equipartition between the particle energy and the magnetic field energy. The equipartition would require a few times larger value of the magnetic field. However, such strong magnetic field could cause efficient synchrotron cooling, reducing

significantly maximum energy of the particles. On the other hand the equipartition does not have to be reached in a compact region of the jet, located at a relatively small distance from the center, where we still may expect the particle acceleration. Note that it is possible to reduce a disagreement between E_e and E_B by considering for example twice as large source and reducing a few times the particle density. This will also significantly decrease the level of the IC emission because this emission is proportional to the square of the particle density. Therefore, the source in equipartition will not produce efficiently the X-ray emission. However, a bigger source needs more time to be created and therefore the particles have more time to be cooled. This reduces significantly γ_{\max} and makes impossible to explain observed level of the emission above 10^{11} Hz. More extended synchrotron source is also optically thin at lower frequencies. The self-absorption break (ν_s) in such spectrum appears below 10^8 Hz which does not agrees with the observations. In other words the bigger source has synchrotron spectrum "shifted" towards lower frequencies.

The radius of the jet knot derived in our first fit is relatively large (356.5 pc), a few times larger than the size of the smallest jet component tightly constrained by the high resolution radio maps (60-70 pc; Kunert-Bajraszewska & Marecki 2007). Therefore in our second fit we assume relatively small radius to be in agreement with the radio observations. The reduced volume of the source must be compensated by increased particle density and/or increased magnetic field strength. However, B cannot be increased significantly because this parameter has direct impact on the maximum energy of the particles. The density can be increased significantly but this will make the source optically thick for the low frequency radio emission, shifting ν_s towards higher frequencies. On the other hand the low frequency radio emission can be produced by more extended structures of the jet. Unfortunately we have only the spectrum of the total emission of 1045+352 without information about the contribution of separated jet components to the total emission. The best fit (Fig. 1b) in this particular case was obtained for $\delta = 1.5$, $B = 3.0 \times 10^{-3}$ G, $K = 19 \text{ cm}^{-3}$ and $R = 2.1 \times 10^{20}$ cm (68 pc). We also calculated values of $\gamma_{\max} = 1.0 \times 10^4$, $U_{\text{rad}}/U_B = 0.21$ and $E_e/E_B = 72.0$. Note that the disproportion between E_e and E_B was slightly reduced. However, further reduction of the source size is not possible. More compact and therefore more dense source would produce efficient X-ray emission, significantly above the observed level.

We assume that well visible excess of the emission in the IR range is produced by dust in the center of 1045+352. Therefore we approximate this emission using a greybody spectrum that differs from a blackbody ($B_{bb}(\nu)$) distribution by a simple factor

$$B_{gb}(\nu) = (1 - e^{-\tau(\nu)})B_{bb}(\nu), \quad (6)$$

where

$$\tau_\nu = \left(\frac{\nu}{\nu_o}\right)^\beta = \left(\frac{\lambda_o}{\lambda}\right)^\beta \quad (7)$$

ν_o is a turn-over frequency (or λ_o , the turn-over wavelength), the frequency at which the source becomes optically thin, and β is the emissivity index of the dust

grains. We use in our calculations $\beta = 2$ that changes index of the power-law part in the spectrum from ν^2 in classical blackbody spectrum to ν^4 in the greybody distribution that better describes thermal emission of the dust. This is in fact the only one difference between the blackbody and greybody spectrum in our approach.

To calculate possible influence of the greybody emission for the inverse-Compton scattering inside the jet component that produces the X-ray emission, we use approximation proposed by Inoue & Takahara (1996). The only one difference between this approximation and our calculations is that we use greybody distribution instead of the blackbody one. According to this approximation the emission is characterized by luminosity of the center (L_{nuc}) and the temperature of the dust (T). Moreover the intensity of the emission in the comoving frame of the source depends on the distance to the center D .

The best spectrum of the observed IR emission was obtained for $\nu_{\text{peak}}L_{\text{nuc}}(\nu_{\text{peak}}) = 8 \times 10^{45}$ erg/s and the dust temperature $T = 50$ K. Moreover, we found that the inverse-Compton scattering of the photons produced by the dust becomes negligible for $D > 2 \times 10^{21}$ cm. Note that the radius of the source is $R = 2.1 \times 10^{20}$ cm thus such relatively large source should not be placed too close to the center and therefore inverse-Compton scattering of the dust photons can be neglected.

The optical data (starlight from the host galaxy) are taken from the SDSS and fitted with the black body curve with a temperature $T = 10^4$ K and $\nu_{\text{peak}}L_{\text{nuc}}(\nu_{\text{peak}}) = 10^{45}$ erg/s. The IC scattering of this additional radiation field appears also negligible for $D > 2 \times 10^{21}$ cm.

The two cases described above and illustrated in Fig. 1a,b show that the high energy emission of a radio-loud BAL quasar can be explained by a simple SSC model. The observed synchrotron emission constrains the free parameters of the model well. Therefore the calculated level of the inverse-Compton emission is also well constrained and appears to be in a good agreement with the observations. In other words, it is difficult to explain the observed synchrotron spectrum of the synchrotron emission and simultaneously to avoid significant emission in the X-ray range due to the SSC scattering. The possibility that the X-ray emission in young GPS sources is produced by a jet was recently discussed (Tengstrand et al. 2009), but there was no straightforward answer so far.

3.2.2. X-ray emission of the corona

We use an accreting corona model derived by Janiuk & Czerny (2000) to model the X-ray emission in 1045+352 (see also other applications of this model: Janiuk et al. (1999); Bechtold et al. (2003)). Following this model, we assume that the (stationary) accretion is ultimately responsible for the broad-band emission, and the flow consists of two media: relatively cold, optically thick disk, and hot, optically thin corona. This model has only three basic parameters: an accretion rate, \dot{M} , a black hole mass, M , and the viscosity parameter, α . The fraction of the energy released in the corona is not a free parameter, but is calculated as a function of radius from the global parameters. All measurable quantities, like the ratio of the disk emission to the coronal emission, the spectral slopes and the extension of the spectrum

into gamma-ray band result from the model, including the trends for the change of these quantities with accretion rate. In the case of limited spectral information a small number of model parameters is a big advantage over the other more complex disk-corona models (e.g. Sobolewska et al. 2004a,b).

We assume that the hot optically thin corona is a two-temperature medium, i.e. the ion temperature is higher than the electron temperature (Shapiro et al. 1967). The loss of gravitational energy by accreting coronal gas is transported directly to ions, while the Coulomb coupling transfers this energy to electrons and finally electrons cool down by the Inverse Compton process. The disk emission provides the source of soft photons for Comptonization, and the amplification factor is defined by the Compton parameter y (Witt et al. 1997).

We assumed a non-rotating black hole so the inner disk radius is located at $3R_{Schw}$ and the Eddington accretion rate is defined using the efficiency of accretion equal to 1/16:

$$\dot{m} = \frac{\dot{M}}{\dot{M}_{\text{Edd}}} = \frac{\dot{M}}{3.52M_8} \quad (8)$$

where $M_8 = M/10^8 M_\odot$ is the black hole mass, and \dot{M} is given in the units of Solar masses per year. The non-rotating black hole model is taken here for simplicity, although in the case of the radio-loud QSOs the rotating black hole is usually considered. The spin of the black hole would result in shifting of the inner radius of the disk-corona system closer to the black hole. However, the coronal emission is dominated by the outermost parts of the corona, and the X-ray spectrum would not change due to the black hole rotation. Therefore the outcome of the modeling is practically unaffected by the value of the black hole spin.

Overall, the model spectra do reproduce the observed AGN spectra, as most of the emission is released from the accretion disk in the UV and soft X-ray bands and some fraction of the total luminosity is emitted in hard X-rays because of Comptonization. These two components, soft and hard, are modelled simultaneously due to the radiative coupling between the disk and corona. The initial input parameters to the model ($M_{BH} = 1 \times 10^8 M_\odot$ and $\dot{m} = 0.36$) were estimated from the spectrum of 1045+352 (Willott et al. 2002). The assumed viscosity parameter, α , was either 0.1 or 0.03. The disk emission was also corrected for the galactic starlight, by means of the thermal emission which peaks at $\log \nu = 14.5$ [Hz]. However, for these initial parameters we did not obtain a satisfactory fit, because the disk luminosity was too high to reproduce correctly the optical emission detected in 1045+352. Also, the coronal emission was too high in X-rays and exceeded the Chandra limits.

By decreasing the accretion rate we obtained a lower flux emitted from the accretion disk, but it didn't help us to fit the optical data. Note that the ratio of the luminosity emitted in the corona with respect to the disk emission is higher for a smaller accretion rate. This is because the Compton cooling of the corona is less efficient due to a lower soft photon flux from the disk, so the electron temperature in the corona can be higher.

The black hole mass does not influence the shape of the spectrum, but a smaller black hole mass helped to shift

the disk peak emission towards somewhat higher energies and better fit the data. To match the optical data we needed to lower the black hole mass to $2 \times 10^7 M_\odot$. This increased the accretion rate, which we had to again decrease and finally we got the best fit with the initial input parameter $\dot{m} = 0.36$.

The spectral shape is affected by both viscosity α and accretion rate \dot{m} . For small viscosity, the relation is roughly monotonic, i.e. the larger \dot{m} , the softer the spectrum. This is because for large \dot{m} the radial extension of the corona is larger. The hard X-rays are generated mainly at large radii from the black hole, because at the outer radius of the corona the fraction of the energy dissipated in the corona is $f_{cor}(r_{out}) \approx 1.0$, while at smaller radii $f_{cor}(r)$ is much lower. For large r_{out} the gravitational energy available for dissipation is smaller, so there is less flux in hard X-rays. Therefore, with the same electron temperature in the corona at r_{out} , we have a much more profound disk emission, that forms the Big Blue Bump and the spectral index is steeper. For a large α , this dependence is not always monotonic. This is because the radial extension of the corona only very weakly depends on viscosity, while the electron temperature decreases with α .

Because of the above complex dependencies, we had to change also the viscosity parameter to fit the data best (Fig. 1b). For a too small viscosity, the corona is rather compact and hot, so the hard X-ray flux was too large. Also, the viscosity cannot be too small: for $\alpha \leq 0.01$ the corona became too small and we could not determine the corona structure. We have applied two values of viscosity parameter to our model: $\alpha = 0.03$ and $\alpha = 0.1$. We found, that for the black hole mass and accretion rate of $M_{BH} = 2 \times 10^7 M_\odot$ and $\dot{m} = 0.36$, both viscosity coefficients give the X-ray flux within the Chandra limit, however a better fit is obtained for the larger value of $\alpha = 0.1$. We note that both these values are plausible for AGN disks. A moderately small value of $\alpha \sim 0.02 - 0.04$ is in agreement with the results of the MHD simulations (Turner 2004; Hirose et al. 2009). On the other hand, the observational constraints for the α parameter give even larger values, of the order of 0.1-0.4 (King et al. 2007), therefore such values are also plausible.

The best model spectrum for 1045+352 is presented in Fig. 1b and with the best parameters: $M_{BH} = 2 \times 10^7 M_\odot$, $\dot{m} = 0.36$ and $\alpha = 0.10$. showing that the observed X-ray emission could be due to both the disk corona and the relativistic jet. However the relativistic jet emission dominates over the corona emission in X-rays. As we discussed in the previous paragraph the jet SSC emission is strong and well constrained by the observed synchrotron spectrum. On the other hand the optical and X-ray data can be affected by the extinction in the source nuclear region and the intrinsic value of the emission of the accretion disk and corona can be higher. Deeper X-ray observations could allow us to estimate the X-ray emission with more accuracy and help us to differentiate between model possibilities.

As we show in the discussion in Sec. 4 the X-ray emission of 1045+352 is very weak comparing to the other radio-loud BAL quasars suggesting a strong absorption. If so the X-ray emission we observe can be mostly due to X-ray emission from the relativistic jet, while the X-ray emission from the corona is absorbed in a large part.

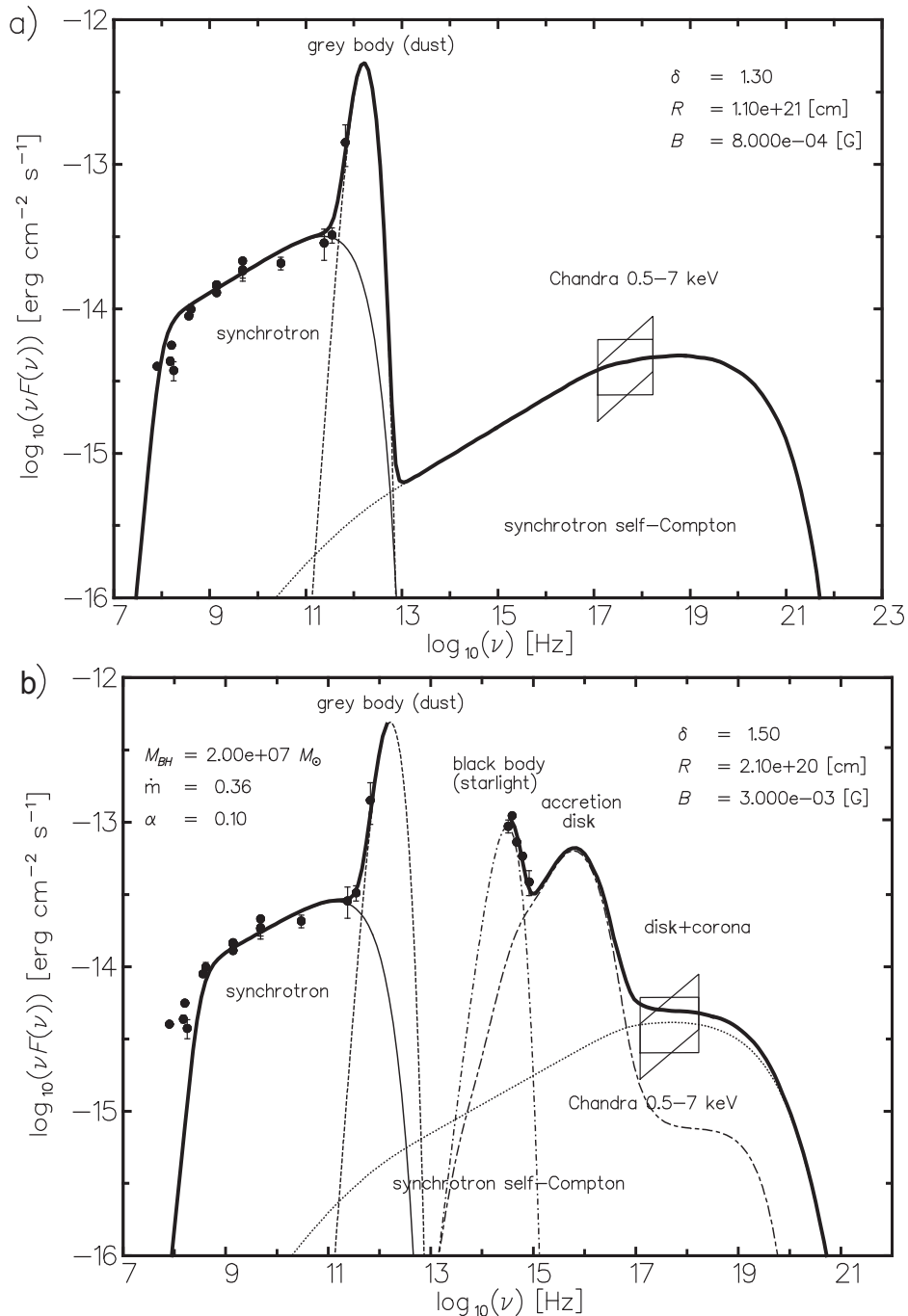


FIG. 1.— Spectral Energy Distribution of 1045+352 based on the data gathered from the literature and SDSS. Our *Chandra* observations are presented as a box: width means 0.5–7 keV range, height is a flux uncertainty, and the box is drawn for $\Gamma=1.7$ and $\Gamma=2$. The curves show the modelled spectral components: synchrotron emission (solid line), and corresponding SSC emission (dotted line), thermal dust emission (dashed line); thermal starlight (dash-dotted line), and comptonized thermal emission from the accretion disk and corona (short-long dashed line). The bold solid line is the sum of the shown spectral components. Since there is a lack of the infrared data the plot is not drawn in that regime. The indicated parameters are: δ - Doppler factor, R - source size, B - magnetic flux, M_{BH} - mass of the black hole, \dot{m} - accretion rate, and α - viscosity parameter. The values of the fluxes are K-corrected.

4. DISCUSSION

Brotherton et al. (2005) made *Chandra* X-ray observations of five radio-loud BAL quasars and noticed that they are X-ray weak relative to similar non-BAL quasars, but brighter than radio-quiet quasars (Fig.2, squares). They interpreted this X-ray weakness as a result of large intrinsic absorption columns. The above suggestions have been confirmed by the X-ray observations of another two radio-loud BAL quasars (Miller et al. 2006;

Schaefer et al. 2006) and it seemed we could draw a separate correlation between an X-ray and radio luminosity for radio-loud BAL quasars. However, recent detections of X-ray bright radio-loud BAL quasars (Wang et al. 2008; Giustini et al. 2008) complicated the picture. We have updated the Brotherton et al. radio to X-ray luminosity plot and added all radio-loud BAL quasars observed in X-rays to date (Giustini et al. 2008; Miller et al. 2006; Schaefer et al. 2006; Wang et al. 2008). We also included our 1045+352 *Chandra* X-ray

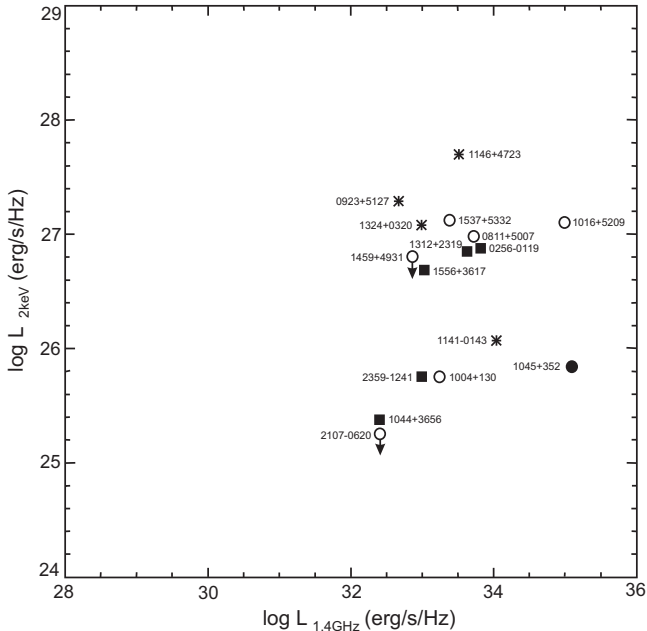


FIG. 2.— Rest frame radio and X-ray luminosities for radio-loud BAL quasars observed in X-rays so far: the five BALs from Brotherton et al. (2005) sample (squares); the first known radio-loud BALQSO with FR II morphology 1016+5209 from Schaefer et al. (2006); large scale hybrid object 1004+130 from Miller et al. (2006); four BALs from Wang et al. (2008), two of them have only upper limit; 1045+352 (this paper); four radio-loud BALs from Giustini et al. (2008)(stars).

data point there. The final Fig.2 contains 16 sources and their properties are gathered in Table 1.

A wide range, three orders of magnitude, of the X-ray luminosities is visible on the plot and the result is similar to that obtained for radio-quiet BAL quasars by Giustini et al. (2008) and Shen et al. (2008). These authors concluded that the large spread in the L_X values is because of the differences in column densities and velocities of the quasar outflows which change with the viewing angle. It has to be put in mind, however, that in the case of X-ray properties of radio-loud BAL quasars we still have a very poor statistics and more observations are needed.

We can measure the orientation angle of radio-loud BALQSOs using radio morphology. This has been done for some of the sources in the sample and the results are given in Table 1. There is a suggestion, based on the radio brightness temperature estimation, that four sources have polar outflows (Wang et al. 2008). For the other three sources with resolved radio structures at 5 GHz (two large scale ones 1004+130 and 1016+5209, and the one CSS object, 1045+352), the angles between the jet axis and the line of sight were estimated (Gregg et al. 2000; Miller et al. 2006; Kunert-Bajraszewska & Marecki 2007) using the core radio-to-optical luminosity ratio defined by Wills & Brotherton (1995). All three have a radio core and one-sided jet suggesting asymmetry, but only in the case of 1045+352 the estimated viewing angle implies beaming. Each of these three sources is located in a very different part of the parameter space in Fig. 2. The beamed 1045+352 with inclination angle $< 30^\circ$ is more than an order of magnitude more luminous in radio than the unbeamed 1004+130 observed at $\sim 45^\circ$ and

both of them have a very similar X-ray luminosity. The unbeamed 1016+5209 at $> 40^\circ$ is an order of magnitude more luminous in X-rays than 1045+352, but both have a very similar radio luminosity. If the position of 1016+5209 in Fig. 2 indicates the amount of absorption then this source should be less absorbed than 1045+352. On the other hand its inclination angle is larger, so the absorption column should be larger than the one in 1045+352. This seems in conflict with the orientation model. The above case is complicated by one more thing: the nature of CSS source 1045+352 is different from that of the two large scale objects. It seems that the jet in 1045+352 is strong and the probable counter-jet is very weak (Kunert-Bajraszewska & Gawroński 2009), but we suspect that there are environmental effects influencing the jet's direction and emission which are difficult to estimate. We treat the value of the viewing angle as a rough estimation.

White et al. (2007) have shown that BALs are not found among the brightest radio-emitting quasars, although below 2 mJy they are systematically brighter than non-BAL objects, with the greatest disparity arising in LoBALs. This may indicate that we are looking closer to the jet axis in quasars with BALs. However the Doppler factor for these sources is rather small (like in the case of 1045+352), and the beaming effect causes inappreciable shift of the sources to the left on the plot (Fig. 2).

4.1. Origin of X-ray emission in BAL quasars

As it has been suggested by some authors the X-ray emission of some BAL quasars can be efficiently absorbed by dense gas close to the BLR region. However, in the case of radio-loud BAL quasars the observed X-ray emission might originate from relativistic jets at the further distance from the core, where there is no shielding gas (Brotherton et al. 2005; Wang et al. 2008). As has been shown in the case of 1004+130 (Miller et al. 2006), the X-ray emission of the radio structure is limited to its very inner part (the radio core and the part of the jet closest to radio core). This is also what we have assumed in our model of X-ray emission of 1045+352. We have shown on the example of 1045+352, that the X-ray emission of the potential young radio jets in BAL quasars can contribute to the observed X-ray emission of the whole source (Fig. 1). It, however, depends on the angle between the jet axis and the line of sight. It is not obvious how the X-ray absorbing gas close/in the BLR region is spaced and if this is a common scheme for all BAL quasars. It could be that more than one scattering path is present there (Lamy & Hutsemékers 2004). If so the radio-jet orientation can give us only an estimation of the X-ray contribution coming from the radio jets, and not necessarily give us the probability of the BAL visibility and the total X-ray emission of the source. In the case of 1045+352 we suspect that the X-ray emission of the corona is strongly absorbed and what we observe is mostly the X-ray emission from the relativistic jet which seems to be very strong (Kunert-Bajraszewska & Marecki 2007).

4.2. Radio properties and evolution of BAL quasars

1045+352 quasar is a CSS radio source with the size of 4.3 kpc. Currently, there are only 17 compact radio-

loud BAL quasars observed with VLBI in the literature (Jiang & Wang 2003; Kunert-Bajraszewska & Marecki 2007; Liu et al. 2008; Montenegro-Montes et al. 2009). About half of them have still unresolved radio structures even in the high resolution observations, the other have core-jet structures indicating some re-orientation or very complex morphology, suggesting a strong interaction with the surrounding medium (Kunert-Bajraszewska & Marecki 2007). All of them are potentially smaller than their host galaxies. The analysis of the spectral shape, variability and polarization properties of some of them shows that they are similar to CSS and GPS objects, and are not oriented along a particular line of sight (Montenegro-Montes et al. 2009). However, it may suggest that BALs are associated with an early stage of the radio source evolution and as has been pointed out by Gregg et al. (2000, 2006) the large scale radio-loud BALQSOs could be objects with restarted activity.

The X-ray properties of GPS/CSS objects and its correlation with the radio data have been recently discussed (Siemiginowska et al. 2008; Tengstrand et al. 2009). According to the authors the correlation between the X-ray and radio luminosities can be different for different group of radio sources. GPS quasars are not absorbed, in contrast to GPS galaxies, which show high X-ray column densities. The radio core luminosities for the GPS galaxies are higher than for FR II sources but their X-ray luminosities are comparable. This can indicate that only the X-ray emission of the very inner part of the radio structure may contribute to the X-ray emission of the whole source. Another suggestion is that making X-ray to radio luminosity correlation we should treat large scale and compact BAL quasars separately.

It has been also mentioned by several authors (Reynolds & Begelman 1997; Kunert-Bajraszewska et al. 2006; Siemiginowska et al. 2008) about the possibility of the intermittent activity in young AGNs, which can be caused by the accretion disk

instabilities (Hatziminaoglou et al. 2001; Janiuk et al. 2004; Czerny et al. 2009). This can lead to the scenario, where we have phases in quasar lifetime dominated alternately by X-ray emission from the base of the radio jet or the accretion disk corona.

5. SUMMARY

We presented *Chandra* X-ray observations and describe spectral properties of a bright radio-loud BAL quasar 1045+352. We suggest that the observed X-ray emission could be due to both the disk corona and the relativistic jet. The X-ray emission due to the jet SSC emission is quite significant and may dominate the X-ray energy range. On the other hand IC scattering emission due to the radiation field produced by dust and stars in the center of the galaxy is negligible in this source. Deeper X-ray observations of 1045+352 will be very useful to constrain possible model's solutions.

We conclude that there is no correlation between the radio and X-ray luminosities present in a sample of radio-loud BAL quasars observed in X-rays to date. A wide range of X-ray emission values indicates a more complicated relationship between X-ray emission, radio emission and orientation based on the radio morphology. There is also still an open question about the evolutionary status of radio-loud BAL quasars. From the radio observations, we may conclude that most of them are compact and probably young radio sources. It is possible then that in the case of radio-loud BAL quasars, BALs are visible until the radio jets escape the host galaxy.

We thank Bożena Czerny for helpful discussions. This research is funded in part by NASA contract NAS8-39073 and *Chandra* Award Number GO8-9115X issued by the Chandra X-Ray Observatory Center, which is operated by the Smithsonian Astrophysical Observatory. This work was supported by the Polish Ministry of Science and Higher Education under grant N N203 303635.

REFERENCES

- Bechtold, J., et al., 2003, ApJ, 588, 119
 Becker, R. H., White, R. L., Gregg, M. D., Brotherton, M. S., Laurent-Muehleisen, S. A.; Arav, N., 2000, ApJ, 538, 72
 Brinkmann, W., Laurent-Muehleisen, S. A., Voges, W., Siebert, J., Becker, R. H., Brotherton, M. S., White, R. L., Gregg, M. D., 2000, A&A, 356, 445
 Brotherton, M. S., Croom, S. M., De Breuck, C., Becker, R. H., Gregg, M. D., 2002, AJ, 124, 2575
 Brotherton, M. S., Laurent-Muehleisen, S. A., Becker, R. H., Gregg, M. D., Telis, G., White, R. L., Shang, Z., 2005, AJ, 130, 2006
 Crusius, A. & Schlickeiser, R. 1986, A&A, 164, L16
 Czerny B., Siemiginowska A., Janiuk A., Nikiel-Wroczyński B., Stawarz L., 2009, ApJ, 698, 840
 Elvis, M. 2000, ApJ, 545, 63
 Gallagher, S. C., Brandt, W. N., Chartas, G., Garmire, G. P., 2002, ApJ, 567, 37
 Gallagher, S. C., Brandt, W. N., Chartas, G., Priddey, R., Garmire, G. P., Sambruna, R. M., 2006, ApJ, 644, 709
 Ganguly, R., Brotherton, M. S., Cales, S., Scoggins, B., Shang, Z., Vestergaard, M., 2007, ApJ, 665, 990
 Garmire, G. P., Bautz, M. W., Ford, P. G., Nousek, J. A., Ricker, G. R., Jr., SPIE, 4851, 28
 Ghisellini, G., Maraschi, L., Treves, A., 1985, A&A, 146, 204
 Ghisellini, G., Guilbert, P., Svensson, R., 1988, ApJ, 334, L5
 Ghosh, K. K. & Punnsly, B., 2007, 661, L139
 Ghosh, K. K. & Punnsly, B., 2008, 674, L69
 Giustini, M., Cappi, M., Vignali, C., 2008, A&A, 491, 425
 Green, P. J., Aldcroft, T. L., Mathur, S., Wilkes, B. J., Elvis, M., 2001, ApJ, 558, 109
 Gregg, M. D., Becker, R. H., Brotherton, M. S., Laurent-Muehleisen, S. A., Lacy, M., White, R. L., 2000, ApJ, 544, 142
 Gregg, M. D., Becker, R. H., de Vries, W., 2006, ApJ, 641, 210
 Hatziminaoglou, E., Siemiginowska, A., Elvis, M., 2001, ApJ, 547, 90
 Hewett, P. C., Foltz, C. B., 2003, AJ, 125, 1784
 Hirose, S., Krolik, J.H., Blaes, O., 2009, ApJ, 691
 Inoue, S., Takahara, F., 1996, ApJ, 463, 555
 Janiuk, A., Czerny, B., Siemiginowska, A., Szczerba, R., 2004, ApJ, 602, 595
 Janiuk, A., Czerny, B., Życki, P. T., 1999, Astro. Lett. and Communications, 38, 227
 Janiuk, A., & Czerny, B., 2000, NewA, 5, 7
 Jiang, D. R., & Wang, T. G. 2003, A&A, 397, L13
 Jones, F. C., 1968, Phys. Rev., 167, 1159
 Kardashev, N. S., 1962, Soviet Astronomy–AJ, 6, 317
 King, A. R., Pringle, J. E., Livio, M., 2007, MNRAS, 376, 1740
 Konigl, A., 1981, ApJ, 243, 700
 Kunert-Bajraszewska, M., Gawroński, M. P., 2009, PoS(IX EVN Symposium)018
 Kunert-Bajraszewska, M., & Marecki, A., 2007, A&A, 469, 437
 Kunert-Bajraszewska, M., Marecki, A., Thomasson, P., 2006, A&A, 450, 945
 Lamy, H., Hutsemékers, D., 2004, A&A, 427, 107

- Liu, Y., Jiang, D. R., Wang, T. G., Xie, F. G. 2008, MNRAS, 391, 246
- McLure, R. J. & Jarvis, M. J., 2002, MNRAS, 337, 109
- Miller, B. P., Brandt, W. N., Gallagher, S. C., Laor, A., Wills, B. J., Garmire, G. P., Schneider, D. P., 2006, ApJ, 652, 163
- Montenegro-Montes, F. M., Mack, K.-H., Benn, C. R., Carballo, R., Gonzalez-Serrano, J. L., Holt, J., Jimnez-Lujn, F., 2009, AN, 330, 157
- Murray, N., Chiang, J., Grossman, S. A., Voit, G. M., 1995, ApJ, 451, 498
- O'Dea, C. P. 1998, PASP, 110, 493
- Polatidis, A. G., & Conway, J. E. 2003, PASA, 20, 69
- Proga, D. & Kallman, T. R., 2004, ApJ, 616, 688
- Reynolds, C. S., & Begelman, M. C., 1997, ApJ, 487, L135
- Schaefer, J. J., Brotherton, M. S., Shang, Z., Gregg, M. D., Becker, R. H., Laurent-Muehleisen, S. A., Lacy, M., White, R. L., 2006, AJ, 132, 1464
- Shapiro, S. L., Lightman, A. P., Eardley, D. M., 1967, ApJ, 204, 187
- Shen, Y., Greene, J. E., Strauss, M. A., Richards, G. T., Schneider, D. P., 2008, ApJ, 680, 169
- Siemiginowska, A., LaMassa, S., Aldcroft, T. L., Bechtold, J., & Elvis, M. 2008, ApJ, 684, 811
- Sobolewska, M. A., Siemiginowska, A., Życki, P. T. 2004, ApJ, 608, 80
- Sobolewska, M. A., Siemiginowska, A., Życki, P. T. 2004, ApJ, 617, 102
- Stawarz, L., Ostorero, L., Begelman, M. C., Moderski, R., Kataoka, J., Wagner, S., 2008, ApJ, 680, 911
- Tengstrand, O., Guainazzi, M., Siemiginowska, A., Fonseca Bonilla, N., Labiano, A., Worrall, D. M., Grandi, P., Piconcelli, E., 2009, A&A, 501, 89
- Turner, N. J., 2004, ApJ, 605, L45
- Wang, J., Jiang, P., Zhou, H., Wang, T., Dong, X., Wang, H., 2008, ApJ, 676, L97
- White, R. L., Helfand, D. J., Becker, R. H., Glikman, E., de Vries, W., 2007, ApJ, 654, 99
- Willott, C. J., Rawlings, S., Archibald, E. N., Dunlop, J. S., 2002, MNRAS, 331, 435
- Wills, B. J., & Brotherton, M. S., 1995, ApJ, 448, L81
- Wills, B. J., Brandt, W. N., Laor, A., 1999, ApJ, 520, L91
- Witt, H. J., Czerny, B., Życki, P. T., 1997, MNRAS, 286, 848
- Young, M., Elvis, M., Risaliti, G., 2009, ApJS, 183, 17
- Zhou, H., Wang, T., Wang, H., Wang, J., Yuan, W., Lu, Y., 2006, ApJ, 639, 716

TABLE 1
BASIC PARAMETERS OF 16 RADIO-LOUD BAL QUASARS.

Source Name	RA h m s	Dec ° ' "	z	$F_{1.4}$	$\log L_{1.4}$	$\alpha_{1.4}^{4.85}$	F_X	$\log L_X$	Γ	α_{ox}	Type	LLS	Radio morph.	Angle
(1)	(2)	(3)	(4)	(5)	(6)	(7)	(8)	(9)	(10)	(11)	(12)	(13)	(14)	(15)
0256-0119	02 56 25.56	-01 19 12.10	2.490	27.56	33.88	0.5	5.04	26.86	1.70	1.90	Hi	<14	S	–
0811+5007	08 11 02.91	50 07 24.57	1.838	24.93	33.55	0.5	12.31	26.95	1.71 *	1.55	Lo	<14	S	P
0923+5127	09 23 45.19	51 27 10.10	2.163	1.79	32.58	0.5	15.60	27.21	1.70	1.59	Hi	<33	S	–
1004+130	10 07 26.10	12 48 56.20	0.240	1126.00	33.26	0.8	96.50	25.78	1.50 *	1.87	Hi	383.5	H	$\sim 45^\circ$
1016+5209	10 16 14.26	52 09 15.45	2.455	176.90	34.99	1.1	96.10	27.13	1.70	1.06(1.19)	Lo	370.0	D	$> 40^\circ$
1044+3656	10 44 59.59	36 56 05.39	0.701	15.00	32.40	0.5	3.41	25.42	1.70	2.0(2.1)	FeLo	<13	S	–
1045+352	10 48 34.25	34 57 24.99	1.604	1051.00	35.13	0.7	1.32	25.84	1.70	1.38(1.88)	Hi	4.3	Cj?	$< 30^\circ$
1141-0143	11 41 11.62	-01 43 06.70	1.266	141.10	33.98	0.6	4.01	26.09	1.70	2.01	Lo	176.6	D	–
1146+4723	11 46 36.88	47 23 13.35	1.895	24.05	33.56	0.5	65.00	27.70	1.70	1.38	Lo	<12	aD?	–
1312+2319	13 12 13.58	23 19 58.64	1.520	44.12	33.74	0.8	15.77	26.87	1.70	1.40	Hi	1.3	Cj?	–
1324+0320	13 24 01.53	03 20 20.60	3.371	1.50	32.88	0.5	3.82	27.03	1.70	1.89	H	<41	S	–
1459+4931	14 59 26.33	49 31 36.86	2.370	4.74	33.06	0.5	4.01	26.82	1.90	1.77	Lo	<45	S	P
1537+5332	15 37 03.94	53 32 19.97	2.403	9.58	33.38	0.5	16.95	27.15	1.31 *	1.73	H	<9	S	P
1556+3517	15 56 33.77	35 17 57.62	1.480	31.72	33.29	0.1	10.56	26.67	1.70	0.8(2.0)	FeLo	<9	S	–
2107-0620	21 07 57.67	-06 20 10.66	0.645	19.61	32.43	0.5	2.86	25.30	1.90	1.93	FeLo	<8	S	P
2359-1241	23 59 53.63	-12 41 47.92	0.870	39.50	33.03	0.5	4.55	25.76	1.70	1.8(2.2)	Lo	<134	S	–

Description of the columns: (1) source name; (2) source right ascension (J2000); (3) source declination (J2000); (4) redshift; (5) total flux density at 1.4 GHz (mJy); (6) log of the radio luminosity at a rest-frame of 1.4 GHz ($\text{erg s}^{-1} \text{Hz}^{-1}$); (7) spectral index between 1.4 and 4.85 GHz; (8) total flux density at 2 keV ($10^{-15} \text{erg s}^{-1} \text{cm}^{-2} \text{keV}^{-1}$) calculated assuming the Galactic absorption and photon index; (9) log of the X-ray luminosity at a rest-frame of 2 keV ($\text{erg s}^{-1} \text{Hz}^{-1}$); (10) photon index, '*' means fitted, in other case - assumed; (11) the optical - X-ray spectral index; quantities in parentheses are calculated using dereddened optical flux; (12) BALQSO subclassification, Hi - HiBAL, Lo - LoBAL, FeLo - FeLoBAL, H - BALQSO for which the MgII spectral region is redshifted outside the SDSS window; (13) largest linear size (h^{-1} kpc), '<' means upper limit of the linear size estimated using deconvolved component major axis angular size from FIRST or NVSS when available or using FIRST beam ($5''4$); (14) radio morphology, S - single means unresolved in available radio image, Cj - core-jet, D - double, aD - asymmetric double, H - hybrid object (FRI/FRII); (15) angle between the jet axis and the observer based on the radio image, P - polar outflow. The information about the radio-loud BAL quasars are gathered from: Brotherton et al. (2005), Giustini et al. (2008), Gregg et al. (2000), Kunert-Bajraszewska & Marecki (2007), Miller et al. (2006), Schaefer et al. (2006), Wang et al. (2008).